Coherence of interacting bosons in optical lattices in synthetic magnetic fields with a large number of subbands

B. Grygiel, K. Patucha, and T. A. Zaleski
Institute of Low Temperature and Structure Research, Polish Academy of Sciences, Okólna 2, 50-422 Wroclaw, Poland
(Received 24 November 2015; published 9 May 2016)

We study the behavior of interacting ultracold bosons in optical lattices in synthetic magnetic fields with wide range of in-cell fluxes $\alpha = p/q$. The problem is similar to the one of an electron moving in a tight-binding scheme in the magnetic field and becomes difficult to tackle for a growing number of magnetic subbands, q. To overcome this, we focus on the interplay of the width, shape, and number of the subbands on the formation of the coherent state of cold bosons. Using the quantum rotor approach, which goes beyond the mean-field approximation, we are able to pinpoint the elements of the band structure, which are the most significant in a proper theoretical description of the synthetic magnetic field in a bosonic lattice system. As a result, we propose a method of reconstruction of the Hofstadter butterfly spectrum by replacing the magnetic subbands with renormalized bands of a square lattice. This allows us to effectively investigate the properties of the studied system for a wide range of magnetic fluxes and their impact on the Mott-insulator–superfluid transition.

DOI: 10.1103/PhysRevA.93.053607

I. INTRODUCTION

The presence of a magnetic field acting on electrons tightly bound in a lattice leads to a complex response of the system known as Hofstadter's butterfly [1,2]. The energetic spectrum splits into magnetic subbands while the precise relation between the number of subbands and value of the magnetic field and also the shape of the bands themselves are nontrivial and nonmonotonic. The strength of the magnetic field is measured by a fraction (α) of a flux through an elementary cell to one flux quantum $\Phi_0 = h/e$. However, in solid-state physics, only very small values of α can be obtained experimentally due to the small size of interatomic distances leading to a description of equally separated Landau levels (e.g., in typical materials $\alpha \approx 1$ would require a magnetic field of $\sim 10^4$–10^5 T).

Recent developments in cooling and trapping techniques of neutral atoms in optical lattices have led to a new field of solid-state-like physics with ultracold gases [3,4]. Counter-propagating laser beams are used to create a spatially periodic pattern of variable light intensity, which due to ac Stark shift is able to trap single atoms in their lowest energy states. Such systems are experimental realizations of Hubbard (fermions) or Bose-Hubbard (bosons) models allowing for precise control of tunneling, interactions between particles, geometry of the lattice, shape of the system, etc. For shallow trapping potential the kinetic energy is dominant and the ground state of the system is the superfluid (SF), characterized by a long-range phase coherence. Increase of the interparticle interactions drives decoherence and strong localization of atoms in lattice sites leading to the Mott-insulating (MI) state [5].

Although the particles trapped in these systems are neutral, they can mimic behavior of charged particles influenced by the magnetic field. It can result from rotation of the system due to correspondence between the Lorentz and Coriolis forces [3]; however, reaching high (synthetic) magnetic fields in this way is not possible. More precise control can be achieved by modification of hopping using phonon-assisted tunneling control [6–10] or lattice shaking [11,12], thus directly implanting a nonvanishing phase φ that atoms acquire while moving from site $\mathbf{r}_i$ to $\mathbf{r}_j$ in the lattice:

$$\varphi = \frac{2\pi i}{\Phi_0} \int_{\mathbf{r}_i}^{\mathbf{r}_j} \mathbf{A} \cdot d\mathbf{l}, \tag{1}$$

with $\mathbf{A}$ being the vector potential of the synthetic magnetic field. In this manner, high values of the magnetic field ($\alpha \sim 1$) can be obtained with arbitrarily engineered vector potentials $\mathbf{A}$ [13]. This additional phase can be related to investigations of a magnetic frustration in systems of Josephson junction arrays [14].

From the theoretical point of view, a description of properties of interacting atoms influenced by a strong (synthetic) magnetic field is highly complicated due to the complex structure of Hofstadter's butterfly. Methods based on the mean-field approximation are not sufficient because they neglect the internal structure of the magnetic energy bands, while only taking into account their total width. Furthermore, the exact shape of the spectrum is known only for a few rational values of $\alpha = p/q$, where $q = 2$, 3, 6, and 8 [15,16]. For smaller values of α the spectrum could be in principle calculated numerically, though it would require a significant effort. To this end, in the present paper we systematically analyze the role of the shape of magnetic subbands in the properties of strongly interacting bosons to propose a simpler method of reconstruction of the spectrum. Moreover, we use the quantum rotor approach, which goes beyond the mean-field approximation by including spatial fluctuations, thus allowing us to properly describe influence of subtleties of magnetic subbands. The approach has been successfully applied to describe quantum phase transitions [17], phase transitions in spin glasses [18], superconducting and magnetic systems [19–21], and Josephson junction arrays [22]. It has been also verified in systems of ultracold atoms in optical lattices by comparison with quantum Monte Carlo calculations [23] or experimental results, e.g., on time-of-flight patterns [24,25]. As a result, we are able to examine the influence of the parameters of the band structure on the formation of the coherent state.

The remainder of the paper is organized as follows. In the first two sections the Bose-Hubbard model and quantum rotor approach are briefly introduced. Section III contains analysis of the band-structure parameters—number of the bands, their flatness, and shape—by employing two test models: Dirac-δ-like bands and a two-band model. This leads to a method of construction of approximated magnetic densities of states (see Sec. IV), which is applied to investigate the phase diagram of the system for a wide range of values of α. Finally, in Sec. V we summarize our results.

II. MODEL

Strongly interacting bosons in optical lattices are well described by the Bose-Hubbard model [26,27], for which the Hamiltonian reads

$$\hat{H} = -\sum_{\langle i,j\rangle} t_{ij}(\hat{a}_i^\dagger \hat{a}_j + \text{H.c.}) + \frac{U}{2}\sum_i \hat{n}_i^2 - \overline{\mu}\sum_i \hat{n}_i, \quad (2)$$

where $\hat{a}_i$ ($\hat{a}_i^\dagger$) is the bosonic annihilation (creation) operator and $\hat{n}_i$ is the particle number operator at the lattice site i. The first term describes tunneling between the nearest-neighboring sites with hopping integral t_{ij}, while the next is related to the on-site repulsive interaction U. Finally, $\overline{\mu} = \mu + U/2$, where μ is the chemical potential, which controls the number of bosons.

A. Method

To proceed, we write the partition function in the path-integral formalism using the Matsubara "imaginary-time" $0 \leqslant \tau \leqslant \beta \equiv 1/k_B T$ (T being temperature) technique [28]:

$$Z = \int [\mathcal{D}\overline{a}\mathcal{D}a] e^{-S[\overline{a},a]}, \quad (3)$$

where the action is defined as

$$S[\overline{a},a] = \int_0^\beta d\tau \left\{ H[\overline{a}(\tau),a(\tau)] + \sum_i \overline{a}_i(\tau)\frac{\partial}{\partial\tau}a_i(\tau)\right\}. \quad (4)$$

The Hamiltonian H is of the same form as in Eq. (2) with operators being substituted by complex fields $\overline{a}_i(\tau)$, $a_i(\tau)$ as a consequence of the path-integral formalism in coherent-state representation [29]. The central point of our approach is a variable transform:

$$a_i(\tau) = e^{i\phi_i(\tau)} b_i(\tau), \quad (5)$$

which allows to isolate U(1) phase symmetry naturally present in the Bose-Hubbard Hamiltonian in the form of phase fields $\phi_i(\tau)$ [19,23,30,31] from the "rotated" bosonic amplitudes $b_i(\tau)$ describing formation of the superfluid density. Since in a strongly interacting bosonic system the phase transition between superfluid and Mott-insulating states is governed by phase ordering, we can restrict ourselves to phase fluctuations and assume that the amplitude fields $b_i(\tau) = b_0 + \delta b_i(\tau) \approx b_0$ following the course of treatment extensively described in Refs. [23,25]. However, in principle, amplitude fluctuations can also be included, which is required, e.g., for investigation of momentum-resolved correlation functions. This leads to the extension of the quantum rotor approach with the Bogoliubov method [25]. The value of b_0 can be obtained from minimalization of the Hamiltonian $H[\bar{a}(\tau),a(\tau)]$:

$$b_0 = \sqrt{\frac{tz + \overline{\mu}}{U}}, \quad (6)$$

where z stands for the coordination number of the lattice. In consequence, the action takes the form of the action of interacting quantum rotors:

$$S[\phi] = \int_0^\beta d\tau \left\{ -2J\sum_{\langle i,j\rangle}\cos(\phi_j - \phi_i) + \sum_i \left(\frac{\dot{\phi}_i^2}{2U} + i\frac{\overline{\mu}}{U}\dot{\phi}_i\right)\right\}, \quad (7)$$

where $J = tb_0^2$ and

$$Z = \int [\mathcal{D}\phi] e^{-S[\phi]}. \quad (8)$$

The integration over ϕ has to be performed carefully, satisfying the boundary condition $\phi_i(\beta) - \phi_i(0) = 2\pi m_i$ with $m_i = 0, \pm 1, \pm 2, \ldots$. The variable transform in Eq. (5) affects the definition of the superfluid order parameter defined as $\Psi_B = \langle a_i(\tau)\rangle$, which factorizes as

$$\Psi_B = \langle b_i(\tau)\rangle\langle e^{i\phi_i(\tau)}\rangle = b_0\psi_B, \quad (9)$$

where $\langle\cdots\rangle$ denotes statistical averaging. As a result, superfluidity requires not only nonzero amplitude b_0, but also phase coherence signaled by nonvanishing ψ_B.

Furthermore, we introduce unimodular fields $\zeta_i(\tau) = e^{i\phi_i(\tau)}$ using the following resolution of unity [25]:

$$1 = \int [\mathcal{D}\overline{\zeta}\mathcal{D}\zeta]\delta[\overline{\zeta}_i(\tau) - e^{-i\phi_i(\tau)}]\delta[\zeta_i(\tau) - e^{i\phi_i(\tau)}]. \quad (10)$$

The partition function can be calculated by weakening the unimodularity condition to be fulfilled only on average [20,32,33],

$$|\zeta_i(\tau)|^2 = 1 \Rightarrow \frac{1}{N}\sum_i |\zeta_i(\tau)|^2 = 1, \quad (11)$$

and representing the Dirac δ with the Laplace transform $\delta(x) = \int d\lambda e^{\lambda x}$, which introduces a Lagrange multiplier λ. As a result, after taking the Fourier transform, the partition function reads

$$Z = \int d\lambda \prod_{\mathbf{k},n} [d\overline{\zeta}_{\mathbf{k}}(\omega_n) d\zeta_{\mathbf{k}}(\omega_n)] e^{N\beta\lambda - S[\overline{\zeta},\zeta]}, \quad (12)$$

where the action

$$S[\overline{\zeta},\zeta] = \frac{1}{\beta N}\sum_{n,\mathbf{k}} \overline{\zeta}_{\mathbf{k}}(\omega_n)\Gamma_\lambda^{-1}(\mathbf{k},\omega_n)\zeta_{\mathbf{k}}(\omega_n), \quad (13)$$

with the propagator

$$\Gamma_\lambda^{-1}(\mathbf{k},\omega_n) = \lambda - J\varepsilon_{\mathbf{k}} + \gamma_n^{-1}, \quad (14)$$

where $\varepsilon_{\mathbf{k}}$ is a dispersion relation and $\omega_n = 2\pi n/\beta$ is the bosonic Matsubara frequency with $n = 0, \pm 1, \pm 2, \ldots$. The propagator contains the phase-phase correlator $\gamma(\tau - \tau') = \langle e^{i\phi(\mathbf{r}\tau) - i\phi(\mathbf{r}\tau')}\rangle$, which is dependent on a single site only. Its

Fourier transform in the limit of $\beta \to \infty$ reads

$$\gamma_n^{-1} = \frac{U}{4}\left\{1 - 4\left[v\left(\frac{\mu}{U}\right) + i\frac{\omega_n}{U}\right]^2\right\}, \tag{15}$$

where $v(x) = x - [x] - 1/2$ and $[x]$ is the floor function, which gives the greatest integer less than or equal to x. In the thermodynamic limit ($N \to \infty$), the Lagrange multiplier can be determined by the saddle-point method $\partial S/\partial\lambda|_{\lambda=\lambda_0} = 0$ with the stationary point value of λ_0. This leads to the equation of state

$$1 - \psi_B^2 = \langle\bar{\zeta}_i(\tau)\zeta_i(\tau)\rangle = \frac{1}{N\beta}\sum_{\mathbf{k},n}\Gamma_{\lambda_0}(\mathbf{k},\omega_n). \tag{16}$$

At criticality and in the phase-ordered state ($\psi_B^2 > 0$) the Lagrange multiplier is fixed by the condition

$$\Gamma_{\lambda_{0c}}^{-1}(\mathbf{k}=0,\omega_n=0) = 0 \;\Rightarrow\; \lambda_{0c} = J\varepsilon_0 - \gamma_0^{-1}, \tag{17}$$

while in the disordered (Mott-insulating) phase it has to be determined from Eq. (16) with $\psi_B = 0$. Combining Eq. (16) with Eq. (17) and introducing density of states (DOS) of the lattice,

$$\rho(x) = \frac{1}{N}\sum_{\mathbf{k}}\delta(x + \varepsilon_{\mathbf{k}}), \tag{18}$$

one arrives at the equation for the critical line, which at $T = 0$ reads

$$1 = \frac{1}{2}\int_{-\infty}^{\infty} dx\, \frac{\rho(x)}{\sqrt{\frac{t}{U}\left(\frac{tz}{U} + \frac{\bar{\mu}}{U}\right)(x - \varepsilon_0) + v^2\left(\frac{\mu}{U}\right)}}. \tag{19}$$

As a result, the shape of the energy bands given by the density of states, $\rho(x)$, is crucial for the critical properties of the system. Because the shape of $\rho(x)$ results directly from the spatial dependence of hopping $J\varepsilon_{\mathbf{k}}$, the presented approach is well suited to analysis of effects of lattice geometry of other modifications of intersite tunneling on the ground state of the Bose-Hubbard model. In contrast, methods based on the mean-field approximation consider only the total bandwidth, ignoring the precise form of $\rho(x)$.

B. Synthetic magnetic field

A synthetic magnetic field can be included in the Bose-Hubbard model by introducing the Peierls phase factor to the hopping integral [2,15], i.e.,

$$t_{ij} \to t_{ij}\exp\left(\frac{2\pi i}{\Phi_0}\int_{\mathbf{r}_i}^{\mathbf{r}_j}\mathbf{A}\cdot d\mathbf{l}\right). \tag{20}$$

This substitution follows from gauge invariance of the Schrödinger equation and leads to modification of the lattice dispersion relation $\varepsilon_{\mathbf{k}}$. As a result, the presence of the magnetic field alters the density of states of the lattice in Eq. (18) and, consequently, the ground state of the system determined by Eq. (19). The Peierls factor breaks the translational invariance of the lattice. To account for that, the magnetic supercell can be introduced, which allows the recovery of the translational symmetry. The size of the supercell results from the chosen gauge as well as the periodicity of the Peierls factor [1]. If α is expressed as a rational fraction p/q, the denominator q determines the size of the supercell, which, however, is still dependent on the choice of the actual gauge. For example, in the Landau gauge $\mathbf{A} = (0, Bx, 0)$ the magnetic supercell is rectangular, containing $q \times 1$ cells of the original lattice. This leads to the dispersion given by Harper's equation [1] with q bands, which is used to calculate the density of states in Eq. (18). As q grows, the size of the supercell rises, making the band structure more complex. In the following, we analyze the influence of the properties of the band structure on the formation of the ground state.

III. ELEMENTS OF THE MAGNETIC BAND STRUCTURE

The primary effect of a magnetic field on energy structure is quenching of kinetic energy. This leads to a change of the number of subbands, their flattening, and modification of their shape. Shift of these parameters with magnetic field in lattice systems is nonmonotonic. In order to understand the influence it has on the ground state of the ultracold bosons, these parameters can be studied separately in effective test models. First, we use an infinitely flat bands scenario to study the role of the number of bands in the regime of flat bands. Next, we consider two bands of finite width to study the role of changing flatness. Finally, we investigate the influence of the internal structure of subbands on the ground state of the system.

A. Infinitely flat bands

In weak magnetic fields ($\alpha \ll 1$), the magnetic cell is very large, containing a significant number of lattice sites. As a result, the system resembles a continuous medium. Hence, we first consider an extreme situation of infinitely flat bands with a density of states given by Dirac δs, i.e., Landau levels. In the case of two subbands, each band contains half of the states of the whole system. Inserting

$$\rho(x) = \frac{1}{2}\left[\delta\left(x - \frac{x_g}{2}\right) + \delta\left(x + \frac{x_g}{2}\right)\right] \tag{21}$$

into Eq. (19) we get the expression for the critical line:

$$1 = \frac{1}{4\left|v\left(\frac{\mu}{U}\right)\right|} + \frac{1}{4\sqrt{\frac{t}{U}\left(\frac{tz}{U} + \frac{\bar{\mu}}{U}\right)x_g + v^2\left(\frac{\mu}{U}\right)}}, \tag{22}$$

where $\varepsilon_0 = -x_g/2$ was introduced in Eq. (19) and x_g is a dimensionless parameter describing the energy gap. In a region where $1/[4|v(\mu/U)|] \geqslant 1$, no solution exists, because the last term in Eq. (22) cannot be negative. As a result, in the range $1/4 \leqslant \mu/U - [\mu/U] \leqslant 3/4$ only the Mott-insulator phase is present for any value of t/U. This appears to be a general feature resulting from the fact that the lowest band has density of states of the form of the Dirac δ, while the size of the Mott-insulator-only region (range in values of μ/U) depends on the weight of this band. For the remaining values of the chemical potential the critical line is defined by Eq. (22). If the number of subbands is increased to n with energy gaps between them equal to $x_g/(n-1)$, the critical state equation

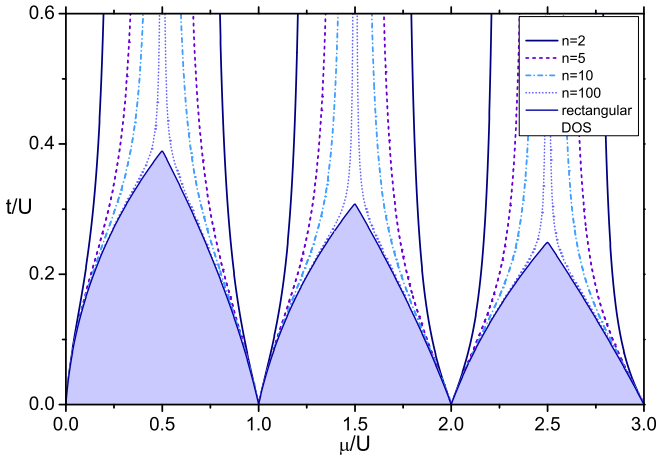

FIG. 1. Phase diagrams of the system with various numbers n of equally separated infinitely flat bands. The narrowing of the Mott-insulator region can be observed as the number of bands increases. The diagram for a rectangular DOS serves as a limiting case of an infinite number of infinitely flat bands ($n \to \infty$).

takes the form

$$1 = \frac{1}{2n\left|v\left(\frac{\mu}{U}\right)\right|} + \sum_{i=2}^{n} \frac{1}{2n\sqrt{\frac{t}{U}\left(\frac{tz}{U}+\frac{\overline{\mu}}{U}\right)\frac{i-1}{n-1}x_g + v^2\left(\frac{\mu}{U}\right)}}. \quad (23)$$

As the number of bands is increased, the Mott-insulator-only region is narrowed (see Fig. 1) and given by $1/2 - 1/(2n) \leqslant \mu/U - [\mu/U] \leqslant 1/2 + 1/(2n)$. This is due to diminishing influence of the lowest flat band on the entire system and directly results from the factor $1/n$ in the first term of Eq. (23) being the weight of the lowest band. In the case of a large number of bands the phase diagram approaches that of a system with a uniform, rectangular density of states, apart from the infinite peaks of critical hopping t/U at the odd multiple of $\mu/U = 1/2$.

B. Finitely flat bands

To investigate the role of finite band flatness we consider a hypothetical scenario of a system consisting of two bands with rectangular density of states and widths equal to d_1 and d_2 for the lower band and higher band, respectively, separated by an energy gap x_g (see Fig. 2). In this case, the integral in Eq. (19) can be calculated exactly and the equation for the critical line reads then

$$1 = \frac{1}{2d_1}\frac{\sqrt{t(tz+\overline{\mu})d_1/U^2 + v^2(\mu/U)} - |v(\mu/U)|}{t(tz+\overline{\mu})/U^2} + \frac{1}{2d_2}\left[\frac{\sqrt{t(tz+\overline{\mu})(d_1+d_2+x_g)/U^2 + v^2(\mu/U)}}{t(tz+\overline{\mu})/U^2} - \frac{\sqrt{t(tz+\overline{\mu})(d_1+x_g)/U^2 + v^2(\mu/U)}}{t(tz+\overline{\mu})/U^2}\right]. \quad (24)$$

Phase diagrams for selected values of flatness of the lower and upper bands, marked as f_1 and f_2, respectively, are presented in Fig. 3. Here, the flatness is defined as a ratio of energy gap to bandwidth, $f_{1,2} = x_g/d_{1,2}$. Through the analysis

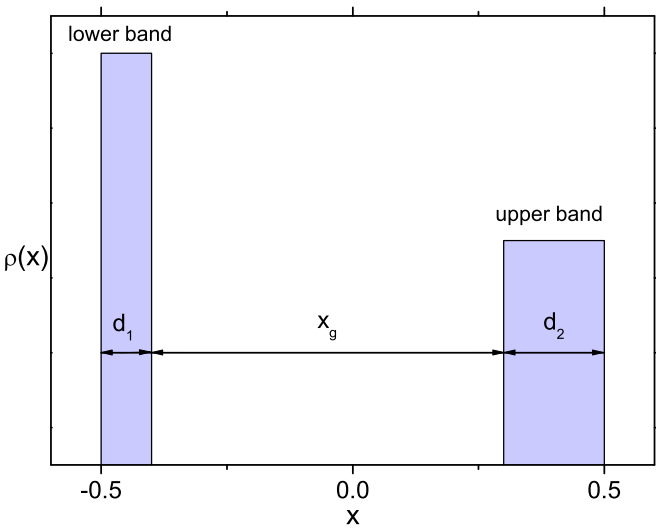

FIG. 2. Illustration of the density of states in a two-band model of finitely flat bands. Bandwidths d_1 and d_2 and gap x_g can be changed freely to investigate which of them has the most pronounced influence on the ground state.

the total bandwidth was kept constant ($d_1 + x_g + d_2 = 1$) in order to avoid the renormalization of the hopping parameter t, allowing for objective comparison of the obtained results. Additionally, while changing the flatness of one of the bands, the width of the other is set constant and equal to 0.1. In consequence the contribution of this band remains constant.

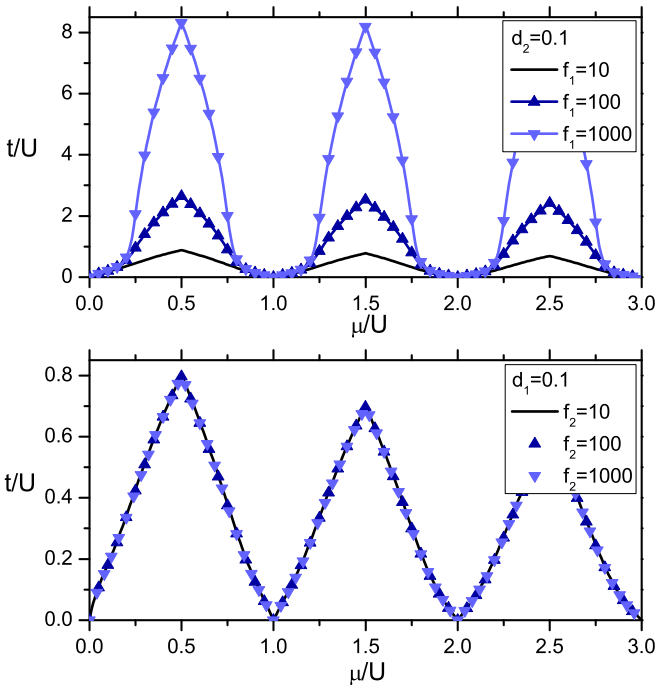

FIG. 3. Phase diagram of superfluid–Mott-insulator transition in the two-band model. The top plot shows changes in the shape of the critical line when the flatness of the lower band, f_1, is changed. A substantial difference in t_c/U occurs near half-integer values of the chemical potential. In the bottom plot the impact of the flatness of the upper band, f_2, on the critical line is presented.

Changing the flatness of the upper band, f_2, has only a slight impact on the shape of the critical line (see Fig. 3). This is due to the fact that the upper band is poorly populated by bosons and thus weakly influences the superfluid–Mott-insulator phase transition. On the other hand, the lower band influences the shape of the phase diagram substantially. For high values of flatness f_1 the phase diagram approaches the limiting behavior of Dirac δ bands (see Sec. III A). The region of the largest increase of the critical hopping corresponds to the MI-only region in the Dirac δ bands model: $1/4 \leqslant \mu/U - [\mu/U] \leqslant 3/4$ (see Sec. III A). As f_1 increases, the superfluid state is suppressed there. This is due to the fact that bosons are not forced by the Pauli exclusion principle to occupy multiple bands. As a result, at low temperatures (or in the ground state) they strongly populate the lowest energy levels. Particularly while the particle density approaches integer values (this occurs for half-integer values of μ/U), the hopping energy in a narrow, flat band is not sufficient to overcome strong repulsive interactions between particles, and the Mott-insulating state is reinforced. Therefore, the influence of the d_1 bandwidth is mostly pronounced for $\mu/U \approx 1/2 + n$.

C. Shape of the bands

In order to assess the influence of the shape of the bands on the critical behavior of ultracold bosons in the regime of flat bands, once again we consider the n-band model (with equally distributed bands) similar to the one investigated in the previous section, when $n = 2$. However, this time we also study how its properties change when the rectangular density of states is replaced by that of a square lattice. Both of the DOS functions exhibit the same behavior around the edges of the band (constant value); however, the square-lattice DOS has a central van Hove singularity, which is of the same type as noncentral van Hove singularities of the magnetic bands in the Hofstadter spectrum. In Fig. 4, a comparison of phase diagrams calculated with rectangular and square lattice DOS for selected values of the lower band flatness is presented. Discrepancies in the shape of the critical line are pronounced mostly near half-integer values of μ/U and they are hardly affected by the flatness of the lowest band, f_1, being still of the same order (around 9%) for a wide range of values of f_1. Finally, we check how the shape of the bands influences the phase diagram, while the number of bands, n, is changed. It appears that, with increasing number of bands, the discrepancies between two DOS functions become smaller and are noticeable in the narrower regions surrounding half-integer values of the chemical potential (see Fig. 5).

The differences in critical hopping between the density of states of a square lattice and the rectangular DOS result from a different distribution of the band weight, which leads to distinct values of DOS functions at ε_0 (for rectangular DOS it is about 1.5 times greater than for the square lattice). However, with increasing number of bands this effect is suppressed due to diminishing impact of the lowest band. These results are consistent with conclusions from Sec. III A.

IV. APPROXIMATED MAGNETIC DENSITY OF STATES

In the previous section it was shown that the number of subbands, but also, most importantly, the width of the lowest bands, has the most significant impact on the critical properties of ultracold bosons in an optical lattice. While the shape of subbands and size of energy gaps that separate them are important, they can be in principle treated less rigorously. However, the energy gaps are intrinsically connected with the widths of subbands (they both sum to the total width of the band structure) so they have to be treated on equal footing, thus leaving the shape of the bands to be simplified. As a result, complicated densities of states obtained from solving Harper's equation can be replaced by simpler, approximated functions, where the structure of energy levels is reproduced exactly but the shape of subbands is selected in such a way that it mimics the original shape of the magnetic subbands, simultaneously lowering computational cost. To this end, we use an appropriately scaled square-lattice density of states for each subband, since it exhibits a central van Hove singularity of the same type as noncentral singularities in magnetic bands.

As a result, the key point of the proposed approximation is to properly determine the energy gaps and bandwidths, which requires solving Harper's equation at two points of the Brillouin zone. Then densities of states of a square lattice

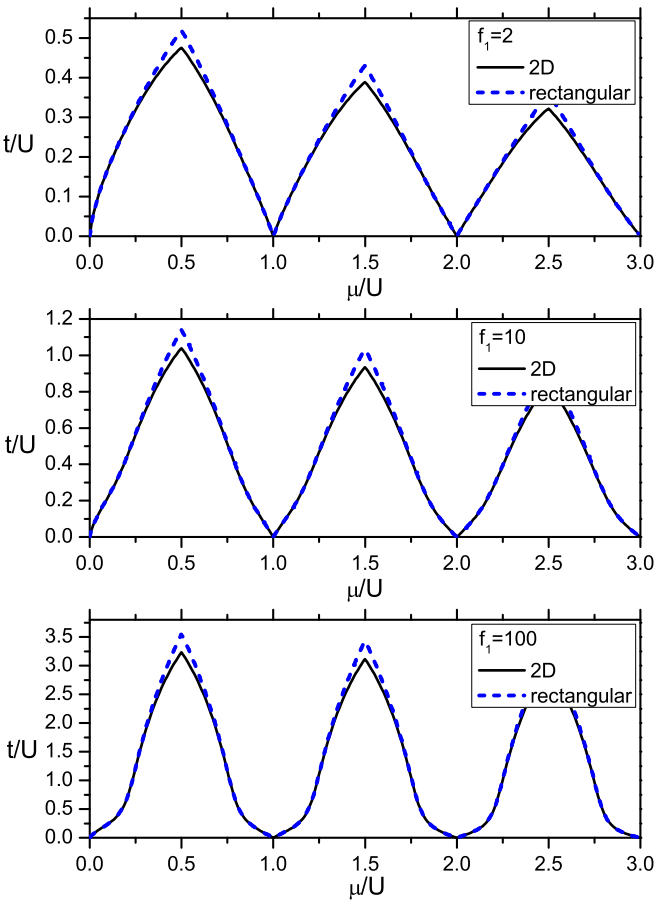

FIG. 4. Comparison of phase diagrams of superfluid–Mott-insulator transition in the two-band model for two different shapes of bands (black solid line, density of states of a square lattice; blue dashed line, rectangular density of states). From top to bottom, the flatness f_1 of the lower band increases. Although the shape of the critical lines is affected by f_1, the behavior around half-integer values of μ/U stays roughly the same.

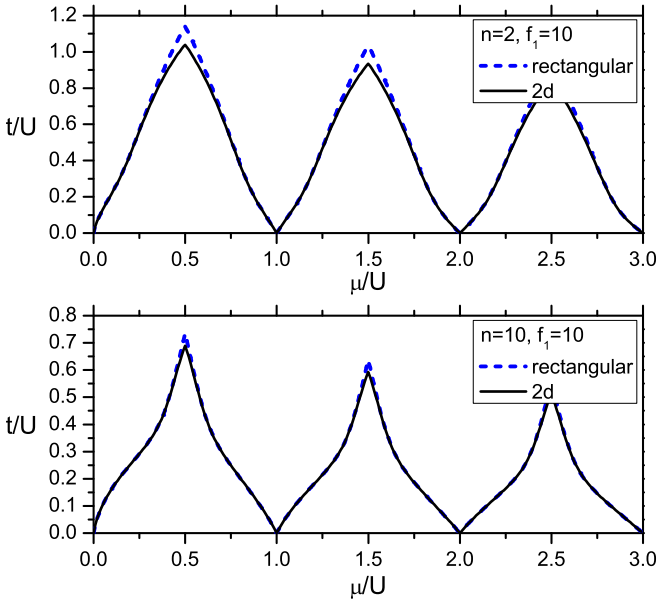

FIG. 5. Comparison of phase diagrams of the superfluid–Mott-insulator transition in the n-band model for two different shapes of bands (black solid line, density of states of a square lattice; blue dashed line, rectangular density of states). With increasing number of bands, n (top, $n = 2$; bottom, $n = 10$), the differences are less pronounced.

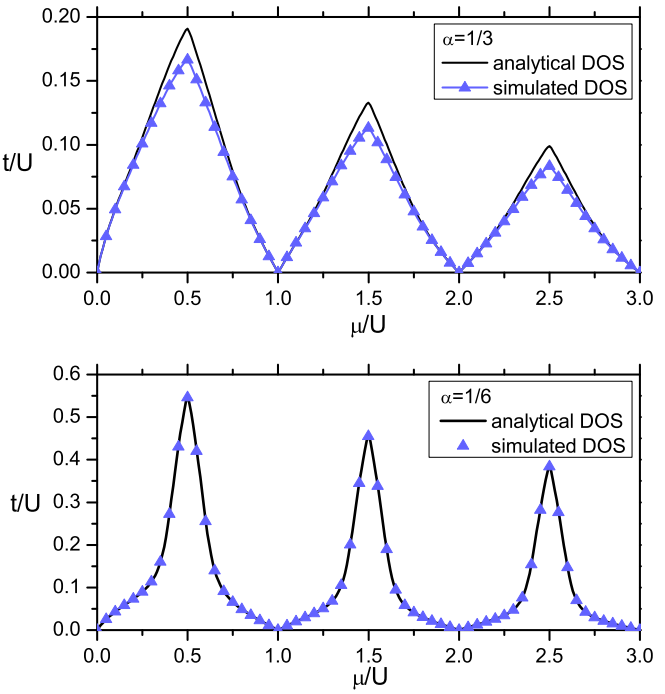

FIG. 6. Comparison of phase diagrams obtained from analytical [16] and simulated magnetic densities of states for two magnetic fluxes: $\alpha = 1/3$ (top) and $\alpha = 1/6$ (bottom). Increasing accuracy can be observed as number of bands, q, increases.

are used to describe each of the subbands. As a result of analysis from the previous section, we expect the largest discrepancies between the approximation and exact solutions to be located around the half-integer values of the chemical potential. Simultaneously, the lower the magnetic field is, the larger is the number of subbands, resulting in more accurate approximation. To check the precision of the proposed method, we compare it with analytical, exact densities of states calculated for small values of α [15,16]. In Fig. 6 we present phase diagrams for $\alpha = 1/3$ and $\alpha = 1/6$. It can be seen that the method becomes more accurate as the number of bands increases. At $\alpha = 1/6$ the phase diagram obtained from a simulated density of states is already in very good agreement with the one obtained from the exact DOS. It is due to the fact that, as the magnetic subbands flatten, the contribution of each of them to the integral in Eq. (19) becomes less dependent on their internal structure, but mostly determined by their total weight and distance from the energy spectrum edge. Therefore, it can be concluded that the approximation works even better for higher values of q.

The application of the method described above allows us to investigate the critical properties of ultracold bosons in an optical lattice for a wide range of fluxes α, corresponding to fractions p/q, where the denominator q is large. In Figs. 7 and 8 we present the dependence of critical hopping t_c/U as a function of magnetic flux α for selected values of the chemical potential μ/U. For comparison, we additionally present the behavior of the inverse of the total energy width, $(\Delta E)^{-1}$, of the Hofstadter butterfly spectrum, which represents a mean-field solution [34]. The shape of the critical line is determined by the following factors. First, the critical hopping is scaled by the total Hofstadter energy spectrum width, similarly as in the mean-field approach. Second, flattening of the lowest band increases the critical hopping near half-integer values of the chemical potentials (tips of lobes) in a similar manner as in the case of a two-band model described in the previous section. Finally, the raising number of the bands leads to a diminishing influence of the lowest flat band and as a result makes the tips of the lobes more narrow. This behavior is analogous to that of infinitely flat bands (see Fig. 1).

The number of bands, q, and the flatness of the lowest band influence the critical hopping differently depending on the value of chemical potential μ/U. For μ/U near integer values (e.g., $\mu/U = 0.2$; see Fig. 7) the behavior is simply scaled by the total energy width of the Hofstadter butterfly and is weakly affected by the number of bands and flatness. As μ/U approaches half-integer values, the number of bands starts to play an important role. As can be deduced from Sec. III A, the growing number of bands makes the region of high t_c/U (in the vicinity of $\mu/U - [\mu/U] = 1/2$) more narrow. We can consider an example of flux $\alpha = 1/5$, where this region is wider than for, e.g., $\alpha = 1/10$. This leads to a bigger increase of t_c in the former case than for the latter at $\mu/U = 0.4$ (see Fig. 8). When μ/U is exactly a half integer, the values of t_c/U belong to the region of strong MI enhancement (analogous to the MI-only region in Sec. III A), independently of the number of bands. This leads to the effect of the increase of critical hopping with flattening of the bands.

V. SUMMARY

The system of ultracold bosons in optical lattices in a synthetic magnetic field has been studied using the

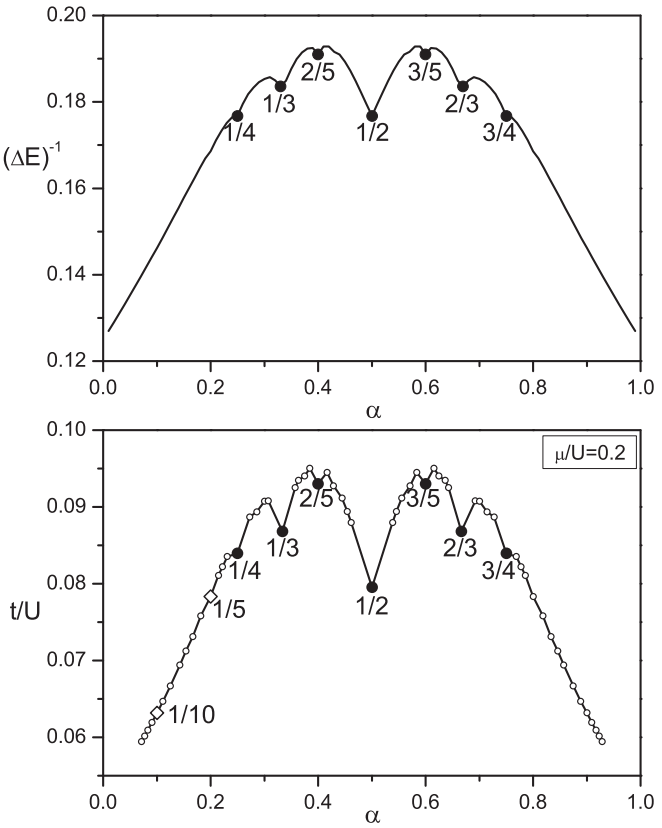

FIG. 7. Top: Dependence of the inverse of total energy width of the Hofstadter butterfly spectrum on the magnetic flux. Bottom: Dependence of critical hopping on magnetic flux for $\mu = 0.2$. Each circle corresponds to a separate value of $\alpha = p/q$ with q up to 13. Reconstructed DOS were used except for $q = 2,3,4$ for which analytical results are easily obtainable. Solid circles indicate characteristic points in the Hofstadter butterfly spectrum. Diamonds correspond to values of $\alpha = 1/5$, $1/10$ considered in the text. The lines connecting points are only guides indicating the order of considered discrete values of α.

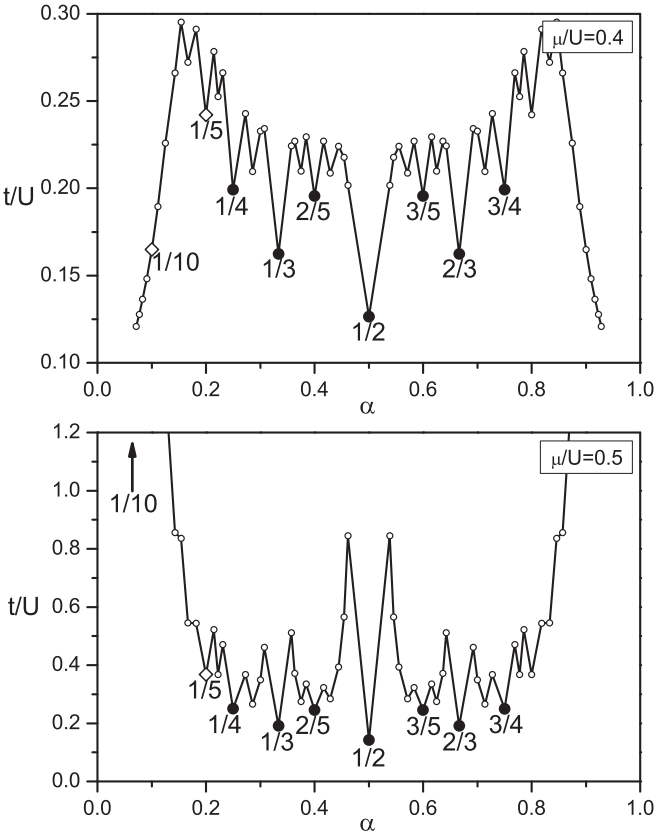

FIG. 8. Dependence of critical hopping on magnetic flux for $\mu = 0.4$ (top) and $\mu = 0.5$ (bottom), depicting non-mean-field behavior. Symbols are used in the same manner as in Fig. 7.

Bose-Hubbard model. The artificial gauge fields have been introduced by Peierls substitution, which affects hopping of atoms. Using the quantum rotors approach the ground state of the system has been determined. The method used includes spatial correlations, which yield the calculated critical line to be not only dependent on the total width of the magnetic bands and the number of the nearest neighbors, but also on subtleties of the complicated structure of the Hofstadter butterfly spectrum. In this sense, the approach goes beyond the mean-field approximation (for details, see Ref. [35]) and allows for analysis of the influence of the shape of the magnetic band structure on the critical properties of the system. The number of bands and the flatness of the lowest bands (being ratios between bandwidths and energy gaps that separate them) have been found as the most crucial elements that affect the formation of the coherent state. This has led to a method of substitution of complicated magnetic densities of states for fluxes $\alpha = p/q$ with large q, which are difficult to be calculated [36], by simpler, approximated form, which still captures the essential physics of the system. This allowed us to determine and explain the phase diagram of the Bose-Hubbard model in a synthetic magnetic field for a wide range of magnetic fluxes. It should be also noted that strong uniform artificial magnetic fields ($\alpha = 1/2$) have already been realized in ultracold atomic systems in optical lattices [10]. Parameters of the Bose-Hubbard model t/U can be estimated using typical experimental quantities from the formula $t/U = \lambda_l \exp(-2\sqrt{V_0/E_R})/(\sqrt{2}\pi a_s)$ (where V_0 is the potential depth, E_R is the recoil energy, λ_l is the laser light wavelength, and a_s is the scattering length) [37]. Finally, in the experimental setups, apart from the periodic landscape of the optical lattice, additional trapping potentials are usually introduced. As a result, systems lose their translational symmetry. The quantum rotor approach used in the present paper requires spatial homogeneity and the infinitely large lattice to work (thermodynamic limit). However, an external trap leads to a spatial change of the chemical potential. Results of the quantum rotor approach can be averaged over that range of the chemical potential to accommodate the presence of the trap, as in Ref. [25].

[1] P. G. Harper, Proc. Phys. Soc. A **68**, 874 (1955).

[2] D. R. Hofstadter, Phys. Rev. B **14**, 2239 (1976).

[3] I. Bloch, J. Dalibard, and W. Zwerger, Rev. Mod. Phys. **80**, 885 (2008).
[4] C. Pethick and H. Smith, *Bose-Einstein Condensation in Dilute Gases* (Cambridge University Press, Cambridge, U.K., 2002).
[5] M. Greiner, O. Mandel, T. Esslinger, T. W. Hänsch, and I. Bloch, Nature (London) **415**, 39 (2002).
[6] D. Jaksch and P. Zoller, New. J. Phys. **5**, 56 (2003).
[7] A. R. Kolovsky, Europhys. Lett. **93**, 20003 (2011).
[8] M. Aidelsburger, M. Atala, M. Lohse, J. T. Barreiro, B. Paredes, and I. Bloch, Phys. Rev. Lett. **111**, 185301 (2013).
[9] H. Miyake, G. A. Siviloglou, C. J. Kennedy, W. C. Burton, and W. Ketterle, Phys. Rev. Lett. **111**, 185302 (2013).
[10] C. J. Kennedy, W. C. Burton, W. C. Chung, and W. Ketterle, Nat. Phys. **11**, 859 (2015).
[11] G. Jotzu, M. Messer, R. Desbuquois, M. Lebrat, T. Uehlinger, D. Greif, and T. Esslinger, Nature (London) **515**, 237 (2014).
[12] J. Struck, M. Weinberg, C. Ölschläger, P. Windpassinger, J. Simonet, K. Sengstock, R. Höppner, P. Hauke, A. Eckardt, M. Lewenstein, and L. Mathey, Nat. Phys. **9**, 738 (2013).
[13] S. Powell, R. Barnett, R. Sensarma, and S. Das Sarma, Phys. Rev. A **83**, 013612 (2011).
[14] R. Fazio and H. van der Zant, Phys. Rep. **355**, 235 (2001).
[15] T. P. Polak and T. K. Kopeć, Phys. Rev. A **79**, 063629 (2009).
[16] T. A. Zaleski and T. P. Polak, Phys. Rev. A **83**, 023607 (2011).
[17] S. Sachdev, *Quantum Phase Transitions* (Cambridge University Press, Cambridge, U.K., 2011).
[18] J. Ye, S. Sachdev, and N. Read, Phys. Rev. Lett. **70**, 4011 (1993).
[19] T. K. Kopeć, Phys. Rev. B **70**, 054518 (2004).
[20] T. A. Zaleski and T. K. Kopeć, Phys. Rev. B **62**, 9059 (2000).
[21] H. Chamati, E. S. Pisanova, and N. S. Tonchev, Phys. Rev. B **57**, 5798 (1998).
[22] F. P. Mancini, P. Sodano, and A. Trombettoni, Phys. Rev. B **67**, 014518 (2003).
[23] T. P. Polak and T. K. Kopeć, Phys. Rev. B **76**, 094503 (2007).
[24] T. P. Polak and T. A. Zaleski, Phys. Rev. A **87**, 033614 (2013).
[25] T. A. Zaleski and T. K. Kopeć, Phys. Rev. A **84**, 053613 (2011).
[26] D. Jaksch, C. Bruder, J. I. Cirac, C. W. Gardiner, and P. Zoller, Phys. Rev. Lett. **81**, 3108 (1998).
[27] M. P. A. Fisher, P. B. Weichman, G. Grinstein, and D. S. Fisher, Phys. Rev. B **40**, 546 (1989).
[28] A. L. Fetter and J. D. Walecka, *Quantum Theory of Many-Particle Systems* (McGraw-Hill, San Francisco, 1971).
[29] H. Kleinert, *Path Integrals in Quantum Mechanics, Statistics, Polymer Physics, and Financial Markets* (World Scientific, Singapore, 2006).
[30] S. Florens and A. Georges, Phys. Rev. B **66**, 165111 (2002).
[31] D. Pesin and L. Balents, Nat. Phys. **6**, 376 (2010).
[32] T. Vojta, Phys. Rev. B **53**, 710 (1996).
[33] T. M. Nieuwenhuizen, Phys. Rev. Lett. **74**, 4293 (1995).
[34] M. Ö. Oktel, M. Niţă, and B. Tanatar, Phys. Rev. B **75**, 045133 (2007).
[35] T. A. Zaleski and T. K. Kopeć, Physica B **456**, 244 (2015).
[36] J. Xu and Q. Gu, Phys. Rev. A **85**, 043608 (2012).
[37] W. Zwerger, J. Opt. B: Quantum Semiclass. Opt. **5**, S9 (2003).